Research Square

Preprints are preliminary reports that have not undergone peer review.
They should not be considered conclusive, used to inform clinical practice,
or referenced by the media as validated information.

Noncontrast Multiparametric MRI Adds Value to Preoperative Peritoneal Cancer Index Assessment in Pseudomyxoma Peritonei: Comparison with Contrast-enhanced CT

Dong BAI
Aerospace Center Hospital
Ruiqing Ma
Aerospace Center Hospital
Chong Wang
Aerospace Center Hospital
Hongjiang Wei
Aerospace Center Hospital
Mengyu Cheng
Aerospace Center Hospital
Jiawei Fan
Aerospace Center Hospital
Wenjuan Liu
Aerospace Center Hospital
Zhiqun Wang
439387525@qq.com
Aerospace Center Hospital

Research Article

Keywords: Pseudomyxoma peritonei, Peritoneal cancer index, Multiparametric MRI, CT, Cytoreductive surgery

Posted Date: November 4th, 2026

DOI: https://doi.org/10.21203/rs.3.rs-11128803/v1

License: This work is licensed under a Creative Commons Attribution 4.0 International License.
Read Full License

Additional Declarations: No competing interests reported.

Abstract

Purpose

To compare noncontrast multiparametric MRI (mpMRI) and contrast-enhanced CT (CECT) for agreement with intraoperative peritoneal cancer index (PCI) and detection of key imaging features in pseudomyxoma peritonei (PMP).

Materials and Methods

This retrospective study included 40 patients with pathologically confirmed PMP who underwent cytoreductive surgery and preoperative mpMRI and CECT in 2024. Intraoperative PCI across 13 abdominopelvic regions served as the reference standard. Total PCI agreement was assessed using intraclass correlation coefficients (ICCs) and Bland–Altman 95% limits of agreement (LoA), with analyses stratified by PCI (≤ 20 vs > 20). Regional agreement and sensitivities for key imaging features were also compared.

Results

Forty patients (median age, 60 years; 25 women) were included. mpMRI showed greater agreement with intraoperative total PCI than CECT (ICC, 0.98 vs 0.90; difference, 0.08 [95% CI: 0.05, 0.15]), with narrower LoA (7.1 vs 19.1 points). Agreement remained greater with mpMRI for PCI ≤ 20 (ICC, 0.91 vs 0.58) and PCI > 20 (ICC, 0.95 vs 0.74). mpMRI showed higher regional agreement in 11 of 13 regions after multiple-comparison correction. mpMRI had higher sensitivity for mucinous ascites (100% vs 61%; P = 0.002) and intralesional septation (95% vs 37%; P = 0.002), whereas CECT had higher sensitivity for intralesional calcification (100% vs 0%; P = 0.021).

Conclusion

Noncontrast mpMRI showed greater agreement with intraoperative PCI than CECT and higher sensitivity for mucinous ascites and intralesional septation, whereas CECT better detected intralesional calcification.

Introduction

Pseudomyxoma peritonei (PMP) is a rare disease characterized by progressive accumulation of mucinous ascites and peritoneal dissemination, most commonly resulting from rupture of an appendiceal mucinous neoplasm [1]. Cytoreductive surgery (CRS) combined with hyperthermic intraperitoneal chemotherapy (HIPEC) is an established treatment for selected patients with PMP and can provide long-term survival benefit [2, 3]. The peritoneal cancer index (PCI), which reflects the extent

and distribution of peritoneal disease, is an important factor in determining the feasibility of complete cytoreduction and patient prognosis [2]. Accurate preoperative assessment of PCI is therefore important for surgical planning and patient selection.

Contrast-enhanced CT is routinely used for preoperative assessment of PMP because of its availability and high spatial resolution and can demonstrate characteristic findings such as mucinous ascites, visceral scalloping, omental involvement, and calcification [4]. However, detection of peritoneal implants at CT depends on lesion size and anatomic location. Small-volume disease and involvement of the small bowel and mesentery are particularly challenging to detect and may lead to underestimation of surgical PCI [5, 6]. Furthermore, limited attenuation differences between mucinous implants and surrounding mucinous ascites may hinder delineation of disease extent [6]. MRI provides greater soft-tissue contrast, while diffusion-weighted imaging may improve lesion conspicuity and detection of peritoneal disease [4]. Previous studies have demonstrated the potential of multiparametric MRI for estimating PCI in patients with peritoneal surface malignancies [8–11]. However, prior studies have largely included heterogeneous tumor types or MRI protocols incorporating gadolinium-based contrast material, and evidence specifically evaluating noncontrast multiparametric MRI for preoperative PCI assessment in patients with PMP remains limited [13–15].

The purpose of this retrospective study was to compare noncontrast multiparametric MRI with contrast-enhanced CT for preoperative assessment of PMP, using surgical PCI as the reference standard. We evaluated agreement between imaging-based and surgical PCI and compared the two modalities for depiction of PMP-associated imaging findings.

Materials and Methods

Study Population

This retrospective study was approved by the institutional review board, and written informed consent was obtained from all patients. A consecutive cohort of 40 patients with pathologically confirmed pseudomyxoma peritonei (PMP) who underwent surgery at our institution between January and December 2024 was included. All patients underwent contrast-enhanced abdominopelvic CT and noncontrast multiparametric MRI within 7 days before surgery.

Inclusion criteria were (a) histopathologically confirmed PMP, (b) completion of both CT and MRI within 7 days before surgery, and (c) complete imaging examinations of diagnostic quality. Exclusion criteria were (a) previous major abdominal surgery other than appendectomy, (b) concurrent malignancy, (c) inadequate image quality, or (d) incomplete surgical documentation. Demographic characteristics, serum tumor marker levels, histopathologic grade, and completeness of cytoreduction scores were obtained from the medical records.

Reference Standard

Intraoperative Peritoneal Cancer Index (PCI) served as the reference standard for imaging-based PCI assessment. Before cytoreduction, the peritoneal cavity was systematically evaluated according to the Jacquet and Sugarbaker PCI system and divided into 13 regions (R0–R12) [16]. For each region, the surgeon assigned a lesion-size score according to the largest visible tumor deposit. Regional scores were summed to yield a total PCI ranging from 0 to 39 (Fig. 1). The surgeons were unaware of the imaging-derived PCI scores assigned retrospectively for this study.The reference standard for the six imaging features was established by integrating operative findings and histopathologic examination of resected specimens, where available. Macroscopic features were primarily determined from operative findings, with histopathologic findings used for confirmation when applicable. Histopathologic examination was also used to confirm the diagnosis and pathologic classification of PMP.

CT Examination

All patients underwent standardized multiphase contrast-enhanced abdominopelvic CT within 7 days before surgery using a dual-source CT system (SOMATOM Force; Siemens Healthineers). Patients fasted for 8 hours before the examination. For bowel distention, 20 mL of diatrizoate meglumine was diluted in 1500 mL of water and administered orally in three 500-mL portions before CT.

The scanning range extended from the diaphragmatic dome to the pubic symphysis. Acquisition parameters included a tube voltage of 120 kVp, tube current of 200–250 mA, section thickness and interval of 5 mm, and pitch of 1.375. Nonionic iodinated contrast material (75–100 mL; 350 mg I/mL) was administered intravenously at 2.5–3.0 mL/sec. Arterial-, portal venous–, and delayed-phase images were acquired at 25–30 seconds, 65–70 seconds, and approximately 15 minutes after contrast material injection, respectively. Axial images were additionally reconstructed at a section thickness of 1.25 mm.

Non-contrast Multiparametric MRI

Noncontrast multiparametric MRI was performed within 72 hours after CT and before surgery using a 3.0-T system (MAGNETOM Skyra; Siemens Healthineers) with an 18-channel body phased-array coil. No gadolinium-based contrast material was administered. The imaging range extended from the diaphragmatic dome to the pubic symphysis.

The protocol included axial, coronal, and sagittal T2-weighted half-Fourier acquisition single-shot turbo spin-echo imaging, with spectral attenuated inversion recovery fat suppression for the axial acquisition; axial noncontrast T1-weighted volumetric interpolated breath-hold examination imaging; and respiratory-triggered axial single-shot echo-planar diffusion-weighted imaging with b values of 50 and 800 sec/mm². Apparent diffusion coefficient (ADC) maps were generated using a monoexponential model from the two b values. Detailed acquisition parameters are provided in Table 1.

Table 1
MRI Acquisition Parameters

Parameter	T2-weighted HASTE	T1-weighted VIBE	DWI(single-shot EPI)
Imaging plane	Axial, coronal, sagittal	Axial	Axial
TR(ms)	1200	4.0	6800
TE(ms)	90	1.9	68
Flip angle(°)	150	10	90
FOV(mm×mm)	380 × 380	380 × 304	380 × 380
Acquisition matrix	320 × 256	256 × 205	192 × 156
Slice thickness(mm)	4	3	4
Slice gap(mm)	0	0	0
Number of excitations (NEX)	2	1	4
GRAPPA	2	2	2
Fat suppression	SPAIR*	Dixon	SPAIR
Motion management	Breath-hold	Breath-hold	Respiratory triggering
b-value(sec/mm²)	—	—	50 / 800

Note:—DWI = diffusion-weighted imaging, EPI = echo-planar imaging, HASTE = half-Fourier acquisition single-shot turbo spin echo, SPAIR = spectral attenuated inversion recovery, VIBE = volumetric interpolated breath-hold examination. GRAPPA was used for parallel imaging with an acceleration factor of 2 for all sequences.*If SPAIR was used only for the axial T2-weighted acquisition, specify: “SPAIR for axial acquisition; no fat suppression for coronal and sagittal acquisitions.”

Image Analysis

Two board-certified abdominal radiologists with 5 and 8 years of experience independently reviewed all CT and MRI examinations while blinded to operative and histopathologic findings. CT and MRI examinations were evaluated in separate reading sessions in randomized order, with a 2-week washout interval between modalities to minimize recall bias.

For each examination, the readers independently assigned regional lesion-size scores and total PCI according to the radiologic segmentation boundaries proposed by Tops-Welten et al. [17] and the Sugarbaker scoring system, using the same 13-region segmentation and lesion-size criteria as the intraoperative reference standard. Interreader agreement was assessed from the initial independent readings. Disagreements were resolved by consensus; unresolved cases were adjudicated by a third

abdominal radiologist with more than 10 years of experience. Consensus or adjudicated scores were used for comparison with the reference standard.

Before image review, the readers participated in a calibration session to standardize predefined criteria for six imaging features: (a) mucinous ascites, defined as fluid with higher attenuation than simple fluid at CT and high signal intensity on T2-weighted images and high-b-value diffusion-weighted images; (b) scalloping, defined as concave impressions along solid-organ surfaces caused by adjacent mucinous deposits; (c) omental cake, defined as diffuse or confluent thickening and infiltration of the greater omentum; (d) intralesional calcification, defined as punctate, curvilinear, or coarse calcific foci; (e) intralesional septation, defined as internal linear septa within a mucinous or peritoneal lesion; and (f) an appendiceal primary lesion, defined as a lesion centered in the appendix showing appendiceal dilatation, a cystic or mucinous mass, mural thickening or enhancement, or mural calcification.

Signal intensity of peritoneal implants on diffusion-weighted images (b = 800 sec/mm²) and ADC maps was visually graded relative to liver parenchyma as markedly hyperintense, mildly hyperintense, or iso- or hypointense.

Statistical Analysis

Statistical analyses were performed using Python 3.12. Continuous variables are reported as medians with interquartile ranges and categorical variables as numbers and percentages.

Agreement of CT- and MRI-derived PCI scores with intraoperative PCI was evaluated separately. For total PCI (range, 0–39), agreement was assessed using a two-way mixed-effects, absolute-agreement, single-measure intraclass correlation coefficient [ICC(A,1)] and Lin concordance correlation coefficient (CCC), with 95% confidence intervals (CIs). Differences in ICC and CCC between MRI and CT were estimated using paired patient-level bootstrap resampling. Bland–Altman analysis was used to estimate bias and 95% limits of agreement (LoA); bootstrap percentile LoA were used for nonnormally distributed differences. A secondary analysis stratified patients according to intraoperative PCI as low burden (≤ 20) or high burden (> 20) [18]. Within each stratum, CT-PCI and MRI-PCI were evaluated using Bland–Altman analysis, absolute PCI error, ICC, and CCC.

For each of the 13 Sugarbaker regions, agreement between imaging-derived and intraoperative ordinal scores (0–3) was assessed using quadratic weighted Cohen κ (κw). Differences between MRI and CT (Δκw) were estimated using paired patient-level bootstrap resampling. Regional analyses were performed overall and within PCI strata. Gwet AC2 was used as a sensitivity measure when κw was not estimable because of insufficient marginal variation.

For each of the six binary imaging features, sensitivity was calculated among reference-standard–positive cases with Wilson 95% CIs. CT and MRI sensitivities were compared using the exact McNemar test; no comparative P value was calculated when no discordant pairs were present.

Interreader agreement before consensus was assessed using ICC(A,1) for total PCI and quadratic weighted κ for regional scores. Bootstrap CIs were based on 5000 patient-level bias-corrected and accelerated resamples. The Benjamini–Hochberg procedure was used to control the false discovery rate across the 13 regional CT-versus-MRI comparisons and the six imaging-feature comparisons. All tests were two-sided, with $P < 0.05$ indicating statistical significance.

Results

Baseline Characteristics

A total of 40 patients with pathologically confirmed pseudomyxoma peritonei were included.

The median age was 60 years (interquartile range [IQR], 52–70 years), and 25 patients (62.5%) were female. Pathologic evaluation showed low-grade PMP in 26 patients (65.0%) and high-grade PMP in 14 patients (35.0%). Completeness of cytoreduction (CC) scores were CC-0, CC-1, CC-2, and CC-3 in 8,5, 4, and 23 patients, respectively. Detailed demographic and clinical characteristics are summarized in Table 2.

Table 2
Patient demographic and clinical characteristics (n = 40)

Characteristic	Value
No. of patients	40
Age (y), median (IQR)	60 [52–70]
Sex, n (%)	
Female	25 (62.5)
Male	15 (37.5)
Pathologic grade, n (%)	
Low-grade PMP	26 (65.0)
High-grade PMP	14 (35.0)
Completeness of cytoreduction score, n (%)	
CCR 0	8 (20.0)
CCR 1	5 (12.5)
CCR 2	4 (10.0)
CCR 3	23 (57.5)
Serum CEA (ng/mL), median (IQR)	13.50 [2.39–45.04]
Serum CA-125 (U/mL), median (IQR)	22.84 [16.68–57.34]
Serum CA-199 (U/mL), median (IQR)	62.69 [10.48–260.24]

Note.— Data are presented as number (percentage) or median (interquartile range). CEA = carcinoembryonic antigen; CA = cancer antigen; CC = completeness of cytoreduction.

Total Peritoneal Cancer Index (PCI) Agreement

MRI-derived total PCI showed greater agreement with intraoperative PCI than CT-derived PCI (Table 3). The ICC was 0.98 (95% CI: 0.97,0.99) for MRI and 0.90 (95% CI: 0.83,0.94) for CT, with an MRI–CT difference of 0.08 (95% CI: 0.05,0.15). Corresponding Lin concordance correlation coefficients were 0.98 (95% CI: 0.97,0.99) for MRI and 0.90 (95% CI: 0.82,0.94) for CT, with a difference of 0.08 (95% CI: 0.05,0.15).

Bland–Altman analysis showed a smaller bias and narrower 95% limits of agreement (LoA) for MRI than for CT (Fig. 2). Mean bias was 0.4 PCI points for MRI and − 1.2 PCI points for CT. The LoA width was 7.1 PCI points for MRI and 19.1 PCI points for CT.

In the burden-stratified analysis, MRI showed greater agreement with intraoperative PCI in both subgroups. In patients with low tumor burden (PCI ≤ 20), the ICC was 0.91 (95% CI: 0.79,0.96) for MRI and 0.58 (95% CI: 0.15,0.79) for CT, with a difference of 0.33 (95% CI: 0.12,0.71). Corresponding LoA widths were 9.6 and 25.5 PCI points, respectively. In patients with high tumor burden (PCI > 20), the ICC was 0.95 (95% CI: 0.91,0.97) for MRI and 0.74 (95% CI: 0.50,0.85) for CT, with a difference of 0.21 (95% CI: 0.09,0.44); corresponding LoA widths were 6.4 and 15.1 PCI points.

Table 3
Agreement of CT- and MRI-derived Total Peritoneal Cancer Index with Intraoperative PCI

Tumor burden	Modality	ICC (95% CI)	CCC (95% CI)	Bias, PCI points	LoA width, PCI points
Overall (n = 40)	CT	0.90(0.83, 0.94)	0.90 (0.82,0.94)	−1.2	19.1
	MRI	0.98 (0.97, 0.99)	0.98(0.97, 0.99)	0.4	7.1*
Low burden, PCI ≤ 20 (n = 14)	CT	0.58 (0.15, 0.79)	0.57 (0.14, 0.78)	−0.9	25.5
	MRI	0.91 (0.79, 0.96)	0.91 (0.78, 0.96)	0.7	9.6
High burden, PCI > 20 (n = 26)	CT	0.74 (0.50, 0.85)	0.73 (0.49, 0.85)	−1.4	15.1
	MRI	0.95 (0.91, 0.97)	0.94 (0.90, 0.97)	0.2	6.4*

Note.— Bias was calculated as imaging-derived PCI minus intraoperative PCI. CCC = Lin concordance correlation coefficient;CI = confidence interval; ICC = intraclass correlation coefficient;LoA = limits of agreement;PCI = Peritoneal Cancer Index.*Percentile-based LoA were used because paired differences were nonnormally distributed.

Regional Agreement

MRI showed higher regional agreement with intraoperative PCI scores than CT in 11 of the 13 Sugarbaker regions after correction for multiple comparisons (Fig. 3). The largest differences in quadratic weighted κ (κw) were observed in R6 (pelvis; Δκw = 0.44), R9 (upper jejunum; Δκw = 0.29), and R10 (lower jejunum; Δκw = 0.31). Differences in R2 and R8 were not statistically significant.

The pattern of regional agreement differed according to tumor burden. In the low-burden group (PCI ≤ 20; n = 14), MRI showed higher κw than CT in R1, R3, R5–R8, and R12 after false discovery rate correction. In the high-burden group (PCI > 20; n = 26), higher κw values for MRI were observed in R4, R5, and R9–R12. In R6 of the high-burden group, κw was not estimable because all reference-standard scores were identical. In R3 of the high-burden group, κw was lower for MRI than for CT (Δκw = − 0.18), although the difference was not statistically significant (FDR-adjusted P = 0.31).

Detection of Imaging Features

MRI had higher sensitivity than CT for mucinous ascites (100.0% [31/31] vs 61.3% [19/31]; FDR-adjusted P = 0.002) and intralesional septation (94.7% [18/19] vs 36.8% [7/19]; FDR-adjusted P = 0.002) (Table 4). In contrast, CT had higher sensitivity for intralesional calcification (100.0% [7/7] vs 0.0% [0/7]; FDR-adjusted P = 0.021). Sensitivity for detection of the primary lesion was 86.7% (13/15) for MRI and 73.3% (11/15) for CT (FDR-adjusted P = 0.50). Both modalities detected all reference-standard–positive cases of omental cake (23/23) and scalloping (24/24)(Fig. 4); because there were no discordant pairs, no comparative P values were reported.

Table 4
Detection Rates of Imaging Features and Comparative Analysis Between CT and MRI

Imaging finding	Reference positive (n)	CT Sensitivity(%) (95%CI)	MRI Sensitivity(%) (95%CI)	P value	FDR-adjusted P value
Mucinous ascites	31	61.3(43.8,76.3)	100.0(89.0,100.0)	< 0.001	0.002
Lesion septation	19	36.8(19.1,59.0)	94.7(75.4,99.1)	0.001	0.002
Intratumoral calcification	7	100.0(64.6,100)	0.0(0.0,35.4)	0.016	0.021
Primary lesion	15	73.3(48.0,89.1)	86.7(62.1,96.3)	0.50	0.50
Omental cake sign	23	100.0(85.7,100.0)	100.0(85.7,100.0)	—	—
Scallop sign	24	100.0(86.2,100.0)	100.0(86.2,100.0)	—	—

Note.— Sensitivity was calculated among reference-standard–positive cases. Values in parentheses are 95% CIs calculated using the Wilson method. P values were calculated using the exact McNemar test and adjusted for multiple comparisons using the Benjamini–Hochberg false discovery rate procedure. No comparative P value was reported when there were no discordant pairs. CI = confidence interval; FDR = false discovery rate.

Discussion

In this paired cohort of 40 patients with pseudomyxoma peritonei (PMP), noncontrast MRI showed greater agreement with intraoperative peritoneal cancer index (PCI) than contrast-enhanced CT (CECT), with a higher ICC (0.98 vs 0.90) and narrower 95% LoA width (7.1 vs 19.1 PCI points). The advantage was maintained in both PCI strata and in 11 of 13 regions. MRI was more sensitive for mucinous ascites (100% [31/31] vs 61% [19/31], P = 0.002) and intralesional septation (95% [18/19] vs 37% [7/19], P = 0.002), whereas CECT was more sensitive for calcification (100% [7/7] vs 0% [0/7], P = 0.021). These

findings suggest that MRI improves PCI assessment by better mapping mucin-dominant, spatially heterogeneous disease.

Accurate characterization of peritoneal disease is central to CRS and HIPEC planning in PMP [19]. PCI is derived from lesion detection and regional scoring across 13 compartments; therefore, regional errors can accumulate into error in total PCI. Bai et al [20] reported limited precision of indirect preoperative PCI estimation, whereas Chua et al [21] found that CT detection of implants was particularly limited in small-intestinal regions. Our paired findings suggest that preoperative discrepancy arises largely from regional lesion mapping rather than uniform global over- or underestimation.

MRI showed narrower LoA than CECT in both PCI strata, with the larger difference at PCI ≤ 20 (9.6 vs 25.5 PCI points). We hypothesize that low-burden PMP contains scattered, thin, or small mucinous deposits with limited CT conspicuity against adjacent fluid. With more extensive disease, larger deposits may be easier to recognize. The low-burden subgroup (n = 14) limits confidence in this interpretation.

The regional pattern supports an imaging-biologic explanation for this finding. PMP is characterized by mucin accumulation and redistribution along peritoneal surfaces [19, 22]. Mucinous deposits may show low attenuation or loculated fluid-like appearance on CT and marked T2 hyperintensity on MRI [23, 24]. The largest MRI-CECT differences occurred in the pelvis and jejunal regions, consistent with difficult CT assessment of small-bowel disease [21]. MRI and DWI also have value for mapping peritoneal disease in colorectal and ovarian malignancies [25, 26], although these findings should not be directly extrapolated to PMP.

Our imaging experience suggests that DWI behaves differently in PMP than in more cellular peritoneal metastases. High-b-value DWI can improve peritoneal lesion conspicuity [27]. PMP contains variable amounts of extracellular mucin and neoplastic epithelium, including lesions with little or no identifiable epithelium [22]; many mucinous deposits in our experience therefore showed only mildly increased high-b-value signal. T2-weighted imaging appeared more sensitive for mucinous material, but T2 hyperintensity alone could not reliably distinguish deposits from mucinous ascites. Morphology was therefore critical: organized deposits often appeared tense, irregular, or mass-forming, whereas free mucinous fluid lacked a defined mass effect. High-b-value DWI provided complementary lesion-to-fluid contrast because fluid was often low signal while deposits remained mildly hyperintense. Thus, in PMP, DWI may contribute less by demonstrating classic diffusion restriction than by complementing T2-weighted morphology. A prior PMP report showed septa on lower-b-value DWI but not at b = 1000 s/mm² [28]. These observations were not quantitatively analyzed and are hypothesis generating.

CECT was uniquely sensitive for calcification, which is better depicted because of the high x-ray attenuation of calcium [29]. Visceral scalloping has been associated with recurrence after complete cytoreduction [30]. PSOGI classification is associated with survival outcomes, although its independent prognostic value remains uncertain [31].

Clinically, MRI may be most useful because it can reduce uncertainty in regions consequential for CRS. Small-bowel and mesenteric involvement can influence feasibility and completeness of cytoreduction [19, 21]. Our rapid HASTE T2-weighted sequence may improve feasibility in patients with extensive abdominal disease by allowing rapid acquisition with reduced sensitivity to physiologic motion, shortening examination time and facilitating cooperation [32]. CECT retains advantages in availability, speed, and calcification detection. Whether improved regional mapping changes surgical selection or cytoreduction remains unknown; recurrence after CRS and HIPEC remains an important concern [33], and HIPEC may benefit selected patients with incomplete cytoreduction [34].

This study had several limitations. First, the retrospective, single-center design and relatively small cohort limited precision, particularly for regional and burden-stratified analyses. Second, patients were recruited from a surgical referral population and may not represent the full spectrum of PMP. Third, regional PCI assessment and imaging-feature evaluation are subject to reader interpretation; interreader reproducibility should be assessed prospectively. Fourth, prospective multicenter studies using standardized imaging and surgical assessment are needed to establish the reproducibility and clinical utility of MRI-based PCI assessment.

In conclusion, noncontrast MRI showed greater agreement with intraoperative PCI than CECT and higher sensitivity for mucinous ascites and intralesional septation, whereas CECT was more sensitive for calcification. The MRI advantage appears to arise from improved regional characterization of mucin-dominant, spatially heterogeneous disease through complementary T2-weighted morphology and DWI. Prospective multicenter studies with quantitative DWI, standardized regional assessment, and surgical endpoints are warranted.

Declarations

Ethics approval and consent to participate

This retrospective diagnostic study was conducted at a single institution in accordance with the ethical principles of the Declaration of Helsinki. The study protocol was approved by the Institutional Review Board, and written informed consent was obtained from all participants.

Consent for publication

Not applicable.

Availability of data and materials

The datasets generated and/or analyzed during the current study are available from the corresponding author on reasonable request.

Competing interests

The authors declare that they have no competing interests or relationships with any companies whose products or services may be related to the subject matter of this article.

Funding

This study was supported by the Cultivation Project of the Beijing Natural Science Foundation–Haidian Original Innovation Joint Fund (Grant No. L2602109).

Authors' contributions

D. B. and R.M. contributed equally to this work. D.B. conceived and designed the study, performed data analysis, prepared the figures, and wrote the main manuscript text. R.M. and C.W. performed the clinical analysis and contributed to the interpretation of the clinical data. H.W., M.C., and J.F. contributed to data collection, data processing, and analysis. W.L. and Z.W. supervised the study, contributed to the study design and interpretation of the results, and revised the manuscript. All authors reviewed and approved the final manuscript.

Acknowledgements

The authors thank all patients who participated in this study and the staff of the Department of Myxoma and the Department of Radiology at Aerospace Center Hospital for their support and assistance.

Authors’information

Dong Bai Email: flybaicai123@163.com, Beijing, China, Aerospace Center Hospital

Ruiqing Ma Email: 584395520@qq.com, Beijing, China, Aerospace Center Hospital

Chong Wang Email: 13935196371@163.com , Beijing, China, Aerospace Center Hospital

Hongjiang Wei Email: 291443027@qq.com, Beijing, China, Aerospace Center Hospital

Mengyu Cheng Email: cmy625729@163.com, Beijing, China, Aerospace Center Hospital

Jiawei Fan Email: 2941952256@qq.com, Beijing, China, Aerospace Center Hospital

Wenjuan Liu* Email: wenjuanliu@163.com, Beijing, China, Aerospace Center Hospital

Zhiqun Wang* Email:439387525@qq.com, Beijing, China, Aerospace Center Hospital

References

1. Smeenk RM, van Velthuysen ML, Verwaal VJ, Zoetmulder FA. Appendiceal neoplasms and pseudomyxoma peritonei: a population based study. Eur J Surg Oncol. 2008;34(2):196–201. 10.1016/j.ejso.2007.04.002.

2. Govaerts K, Lurvink RJ, De Hingh IHJT, Van der Speeten K, Villeneuve L, Kusamura S, Kepenekian V, Deraco M, Glehen O, Moran BJ, PSOGI. Appendiceal tumours and pseudomyxoma peritonei: Literature review with PSOGI/EURACAN clinical practice guidelines for diagnosis and treatment. Eur J Surg Oncol. 2021;47(1):11–35. 10.1016/j.ejso.2020.02.012.
3. Kusamura S, Delhorme JB, Taibi A, Villeneuve L, Deraco M, Dico RL, Glehen O, Moran B. The 2022 PSOGI International Consensus on HIPEC Regimens for Peritoneal Malignancies: Pseudomyxoma Peritonei. Ann Surg Oncol. 2024;31(9):6262–73. 10.1245/s10434-024-15646-6.
4. Jorgenson LC, Wang SS, Grotz TE, Graham RP, Navin PJ, Favazza C, Venkatesh SK, Fidler JL, Fletcher JG, Ehman EC, Sheedy SP. Mucinous Appendiceal Neoplasms and Pseudomyxoma Peritonei: Imaging Features and Current Therapies. Radiographics. 2025;45(6):e240131. 10.1148/rg.240131.
5. Pastier C, De Hingh IHJT, Goéré D. New insights in the management of pseudomyxoma peritonei. J Surg Oncol. 2024;130(6):1316–25. 10.1002/jso.27842.
6. Bai M, Chen J, Xu Y, Feng J, Ma R, Jia H, Xu H, Liang G, Wei H. Bland-Altman agreement analysis between CT predicted and surgical peritoneal cancer index in pseudomyxoma peritonei of appendiceal origin. Sci Rep. 2023;13(1):21520. 10.1038/s41598-023-48975-9.
7. Bai M, Wang S, Liang G, Cai Y, Lu Y, Hou N, Ma R, Xu H, Zhang M. Nomogram to Predict Incomplete Cytoreduction for Pseudomyxoma Peritonei. Ann Surg Oncol. 2022;29(2):885–92. 10.1245/s10434-021-10725-4.
8. Han X, Zhang Q, Zhou N, Ma R, Wang J, Zhai X, Cui B, Lu Y, Liang L. Combined ultrasonography and CT for prognosis and predicting clinical outcomes of patients with pseudomyxoma peritonei. Eur Radiol. 2023;33(4):2800–8. 10.1007/s00330-022-09242-z.
9. Low RN, Barone RM, Gurney JM, Muller WD. Mucinous appendiceal neoplasms: preoperative MR staging and classification compared with surgical and histopathologic findings. AJR Am J Roentgenol. 2008;190(3):656–65. 10.2214/AJR.07.2018.
10. Low RN, Barone RM, Lucero J. Comparison of MRI and CT for predicting the Peritoneal Cancer Index (PCI) preoperatively in patients being considered for cytoreductive surgical procedures. Ann Surg Oncol. 2015;22(5):1708–15. 10.1245/s10434-014-4041-7.
11. Low RN, Barone RM. Combined diffusion-weighted and gadolinium-enhanced MRI can accurately predict the peritoneal cancer index preoperatively in patients being considered for cytoreductive surgical procedures. Ann Surg Oncol. 2012;19(5):1394–401. 10.1245/s10434-012-2236-3.
12. Torkzad MR, Casta N, Bergman A, Ahlström H, Påhlman L, Mahteme H. Comparison between MRI and CT in prediction of peritoneal carcinomatosis index (PCI) in patients undergoing cytoreductive surgery in relation to the experience of the radiologist. J Surg Oncol. 2015;111(6):746–51. 10.1002/jso.23878.
13. Chia CS, Wong LCK, Hennedige TP, Ong WS, Zhu HY, Tan GHC, Kwek JW, Seo CJ, Wong JSM, Ong CJ, Thng CH, Soo KC, Teo MCC. Prospective Comparison of the Performance of MRI Versus CT in the Detection and Evaluation of Peritoneal Surface Malignancies. Cancers (Basel). 2022;14(13):3179. 10.3390/cancers14133179.

14. Laghi A, Bellini D, Rengo M, Accarpio F, Caruso D, Biacchi D, Di Giorgio A, Sammartino P. Diagnostic performance of computed tomography and magnetic resonance imaging for detecting peritoneal metastases: systematic review and meta-analysis. Radiol Med. 2017;122(1):1–15. 10.1007/s11547-016-0682-x.
15. Menassel B, Duclos A, Passot G, Dohan A, Payet C, Isaac S, Valette PJ, Glehen O, Rousset P. Preoperative CT and MRI prediction of non-resectability in patients treated for pseudomyxoma peritonei from mucinous appendiceal neoplasms. Eur J Surg Oncol. 2016;42(4):558–66. 10.1016/j.ejso.2016.01.005.
16. Jacquet P, Sugarbaker PH. Clinical research methodologies in diagnosis and staging of patients with peritoneal carcinomatosis. Cancer Treat Res. 1996;82:359–74. 10.1007/978-1-4613-1247-5_23.
17. Tops-Welten MW, Ewals LJS, van Hellemond IEG, Piek JMJ, Lahaye MJ, De Hingh IHJT, Nederend J, Luyer MDP. Defining region boundaries to assess the peritoneal cancer index on imaging: a Delphi study. Eur Radiol. 2025;35(12):7856–66. 10.1007/s00330-025-11762-3.
18. Chua TC, Moran BJ, Sugarbaker PH, Levine EA, Glehen O, Gilly FN, Baratti D, Deraco M, Elias D, Sardi A, Liauw W, Yan TD, Barrios P, Gómez Portilla A, de Hingh IH, Ceelen WP, Pelz JO, Piso P, González-Moreno S, Van Der Speeten K, Morris DL. Early- and long-term outcome data of patients with pseudomyxoma peritonei from appendiceal origin treated by a strategy of cytoreductive surgery and hyperthermic intraperitoneal chemotherapy. J Clin Oncol. 2012;30(20):2449–56. 10.1200/JCO.2011.39.7166.
19. Lin YL, Xu DZ, Li XB, Yan FC, Xu HB, Peng Z, Li Y. Consensuses and controversies on pseudomyxoma peritonei: a review of the published consensus statements and guidelines. Orphanet J Rare Dis. 2021;16(1):85. 10.1186/s13023-021-01723-6.
20. Bai M, Feng J, Liu J, Li Y, Xu Y, Ma F, Ma R, Liang G, Liu X, Zhao N. Prediction of preoperative peritoneal cancer index for pseudomyxoma peritonei by multiple linear regression analysis. Front Mol Biosci. 2024;11:1512937. 10.3389/fmolb.2024.1512937.
21. Chua TC, Al-Zahrani A, Saxena A, Glenn D, Liauw W, Zhao J, Morris DL. Determining the association between preoperative computed tomography findings and postoperative outcomes after cytoreductive surgery and perioperative intraperitoneal chemotherapy for pseudomyxoma peritonei. Ann Surg Oncol. 2011;18(6):1582–9. 10.1245/s10434-010-1492-3.
22. Carr NJ. New insights in the pathology of peritoneal surface malignancy. J Gastrointest Oncol. 2021;12(Suppl 1):S216–29. 10.21037/jgo-2020-01.
23. Pickhardt PJ, Perez AA, Elmohr MM, Elsayes KM. CT imaging review of uncommon peritoneal-based neoplasms: beyond carcinomatosis. Br J Radiol. 2021;94(1119):20201288. 10.1259/bjr.20201288.
24. Polici M, Palmeri F, Golia E, Parri E, Gentiloni Silveri G, Puglisi F, De Santis D, Zerunian M, Pucciarelli F, Polidori T, Ciolina M, Sammartino P, Laghi A, Caruso D. CT and MR in peritoneal malignancies: pearls and pitfalls at preoperative examination. Insights Imaging. 2025;16(1):171. 10.1186/s13244-025-02060-z.

25. Engbersen MP, Aalbers AGJ, Van't Sant-Jansen I, Velsing JDR, Lambregts DMJ, Beets-Tan RGH, Kok NFM, Lahaye MJ. Extent of Peritoneal Metastases on Preoperative DW-MRI is Predictive of Disease-Free and Overall Survival for CRS/HIPEC Candidates with Colorectal Cancer. Ann Surg Oncol. 2020;27(9):3516–24. 10.1245/s10434-020-08416-7.
26. Tsili AC, Alexiou G, Tzoumpa M, Siempis T, Argyropoulou MI. Imaging of Peritoneal Metastases in Ovarian Cancer Using MDCT, MRI, and FDG PET/CT: A Systematic Review and Meta-Analysis. Cancers (Basel). 2024;16(8):1467. 10.3390/cancers16081467.
27. Ablefoni M, Leonhardi J, Ehrengut C, Mehdorn M, Sucher R, Gockel I, Denecke T, Meyer HJ. Magnetic Resonance Imaging of Peritoneal Carcinomatosis: Evaluation of High b-Value Computed Diffusion-Weighted Imaging. Curr Oncol. 2022;29(7):4593–603. 10.3390/curroncol29070364.
28. Himoto Y, Kido A, Fujimoto K, Kawada K, Kitai T, Sakai Y, Togashi K. A case of pseudomyxoma peritonei: visualization of septa using diffusion-weighted images with low b values. Abdom Radiol (NY). 2016;41(9):1713–7. 10.1007/s00261-016-0697-8.
29. Sun P, Li X, Wang L, Wang R, Du X. Enhanced computed tomography imaging features predict tumor grade in pseudomyxoma peritonei. Quant Imaging Med Surg. 2022;12(4):2321–31. 10.21037/qims-21-976.
30. Hotta M, Minamimoto R, Gohda Y, Tajima T, Kiyomatsu T, Yano H. Pseudomyxoma peritonei: visceral scalloping on CT is a predictor of recurrence after complete cytoreductive surgery. Eur Radiol. 2020;30(8):4193–200. 10.1007/s00330-020-06756-2.
31. Martín-Román L, Hannan E, Faraz Khan M, Müller AS, Shields C, Aird J, Moran B, Mulsow J. Correlation between PSOGI pathological classification and survival outcomes of patients with pseudomyxoma peritonei treated using cytoreductive surgery and HIPEC: national referral centre experience and literature review. Pleura Peritoneum. 2023;8(2):65–74. 10.1515/pp-2023-0001.
32. Tang Y, Yamashita Y, Takahashi M. Ultrafast T2-weighted imaging of the abdomen and pelvis: use of single shot fast spin-echo imaging. J Magn Reson Imaging. 1998 Mar-Apr;8(2):384–90. 10.1002/jmri.1880080218.
33. Yrjönen A, Koskenvuo L, Haapamäki C, Lepistö A. Recurrence after cytoreductive surgery and HIPEC for pseudomyxoma peritonei: A single-center retrospective cohort study. Scand J Surg. 2024;113(2):140–9. 10.1177/14574969231200653.
34. Wang B, Ma R, Shi G, Fan X, Rao B, Xu H. Hyperthermic intraperitoneal chemotherapy in patients with incomplete cytoreduction for appendiceal pseudomyxoma peritonei: a 10-year treatment experience in China. Orphanet J Rare Dis. 2024;19(1):8. 10.1186/s13023-023-02995-w.

Figures

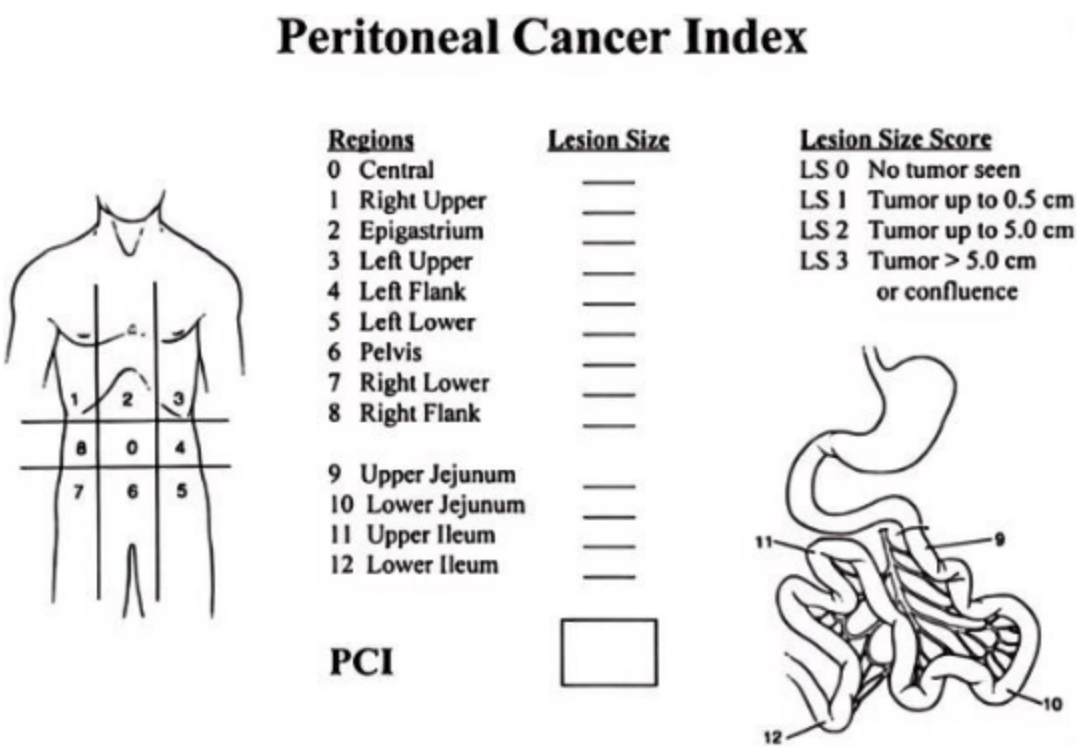


Figure 1

Diagram shows the 13 regions of the peritoneal cancer index (PCI) of Jacquet and Sugarbaker (reference 16): nine abdominopelvic regions (0–8) and four small-bowel regions (9–12), viewed anteriorly. A lesion-size (LS) score of 0–3 is assigned to each region, and the 13 scores are summed to yield a total PCI of 0–39.

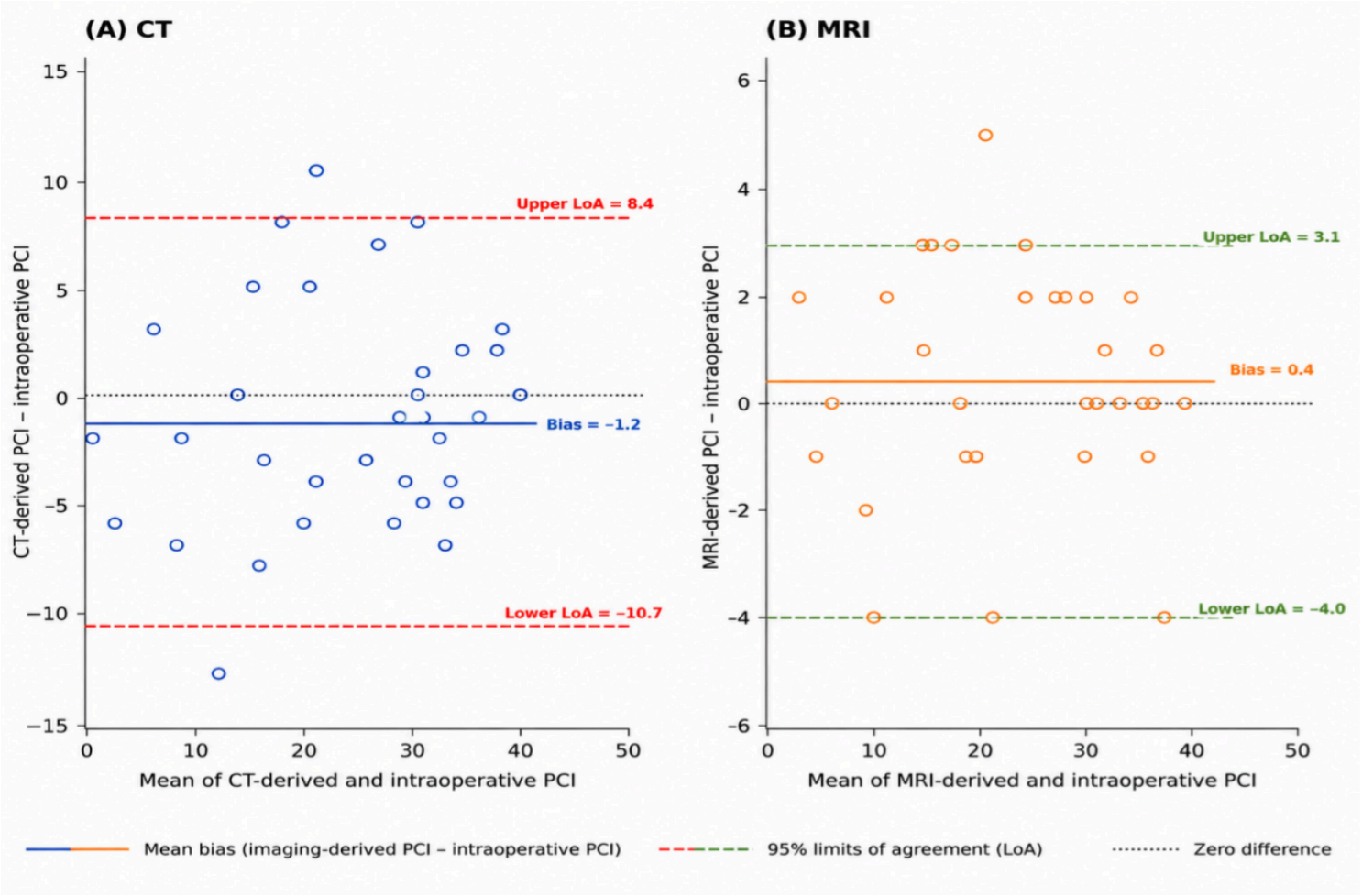


Figure 2

Bland–Altman plots of total Peritoneal Cancer Index (PCI) for (A) CT and (B) MRI compared with intraoperative PCI. The x-axis represents the mean of the imaging-derived and intraoperative PCI scores, and the y-axis represents the difference (imaging-derived PCI minus intraoperative PCI). Solid lines indicate mean bias, dashed lines indicate the 95% limits of agreement (LoA), and dotted lines indicate zero difference.

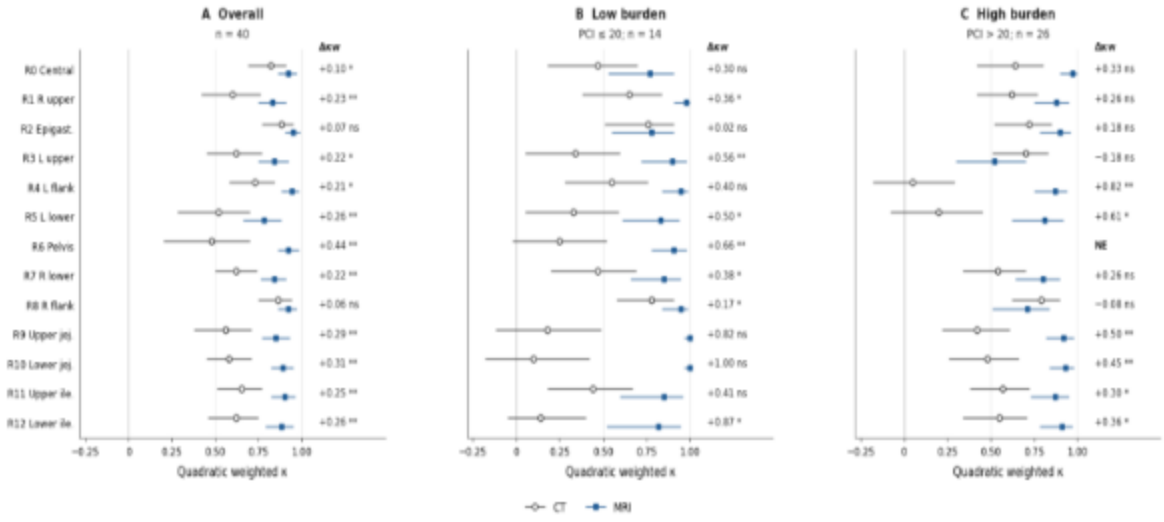


Figure 3

Regional agreement of CT- and MRI-derived scores with intraoperative scores across the 13 Sugarbaker regions in (A) the overall cohort, (B) patients with low tumor burden (reference PCI ≤20), and (C) patients with high tumor burden (reference PCI >20). Circles indicate CT and squares indicate MRI; error bars represent 95% CIs for quadratic weighted κ (κw). Differences are expressed as Δκw (MRI − CT). P values for between-modality differences were adjusted using the Benjamini–Hochberg false discovery rate procedure. In R6 of the high-burden subgroup, κw was not estimable because all reference-standard scores were identical. *Adjusted P < 0.05; **adjusted P < 0.01. NE = not estimable; ns = not significant; PCI = Peritoneal Cancer Index.

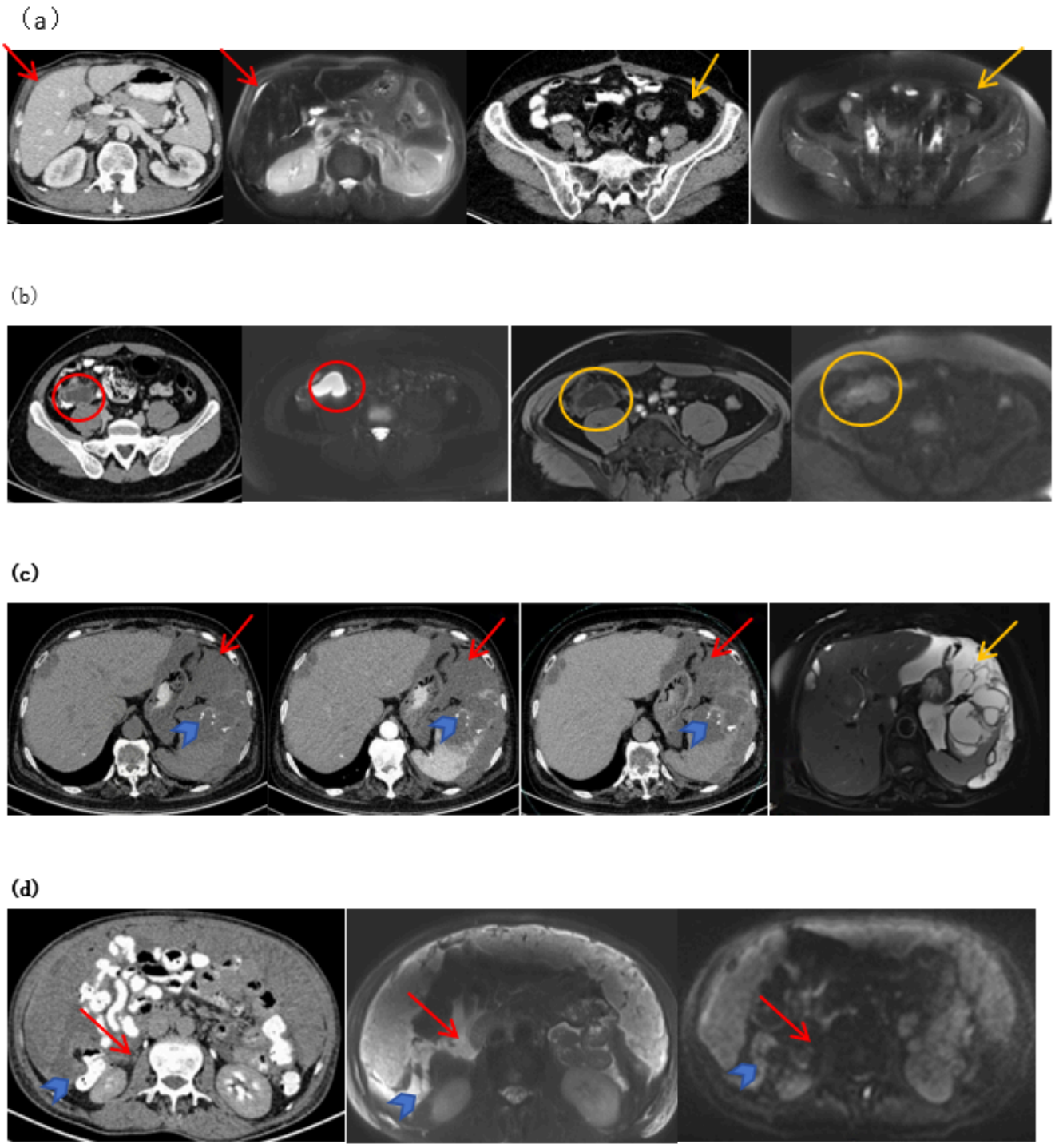


Figure 4

Representative imaging features.(a) Small peritoneal lesions. The first two image pairs show perihepatic lesions (arrows) on CT and MRI. The latter two image pairs show small lesions in the left lower abdominal region (R5) (arrows), which are more conspicuous on MRI. **(b)** Appendiceal primary lesion. Contrast-enhanced CT shows a markedly dilated appendix with mural thickening and enhancement (circle). The lesion is hyperintense on fat-suppressed T2-weighted imaging, hypointense on T1-weighted imaging, and hyperintense on diffusion-weighted imaging (circles).**(c)**Peritoneal lesions with

enhancement, calcification, and septation. Unenhanced, arterial-phase, and delayed-phase CT images show multiple hypoattenuating lesions around the liver, spleen, and stomach with mild delayed enhancement (arrows) and intralesional calcifications (blue arrows). Fat-suppressed T2-weighted imaging shows corresponding hyperintense lesions with internal septations (yellow arrows).**(d)** Mucinous ascites and mucinous tumor. CT shows two low-attenuation lesions (red and blue arrows), both of which are hyperintense on T2-weighted imaging. On diffusion-weighted imaging, the red-arrow lesion is hypointense, whereas the blue-arrow lesion is hyperintense. Operative and histopathologic findings identified the blue-arrow lesion as mucinous ascites and the red-arrow lesion as mucinous tumor.